



Published in final edited form as:

Nat Chem Biol. 2017 September ; 13(9): 943–950. doi:10.1038/nchembio.2420.

A small-molecule allosteric inhibitor of *Mycobacterium tuberculosis* tryptophan synthase

Samantha Wellington^{1,2,3}, Partha P Nag^{1,9}, Karolina Michalska^{4,5,9}, Stephen E Johnston¹, Robert P Jedrzejczak^{4,5}, Virendar K Kaushik¹, Anne E Clatworthy³, Noman Siddiqi⁶, Patrick McCarren¹, Besnik Bajrami¹, Natalia I Maltseva⁴, Senya Combs³, Stewart L Fisher¹, Andrzej Joachimiak^{4,5,7}, Stuart L Schreiber^{1,8}, Deborah T Hung^{1,2,3,*}

¹The Broad Institute, Cambridge, Massachusetts, USA.

²Department of Genetics, Harvard Medical School, Boston, Massachusetts, USA.

³Department of Molecular Biology and Center for Computational and Integrative Biology, Massachusetts General Hospital, Boston, Massachusetts, USA.

⁴Center for Structural Genomics of Infectious Diseases, University of Chicago, Chicago, Illinois, USA.

⁵Structural Biology Center, Biosciences Division, Argonne National Laboratory, Argonne, Illinois, USA.

⁶Harvard T.H. Chan School of Public Health, Boston, Massachusetts, USA.

⁷Department of Biochemistry and Molecular Biology, University of Chicago, Chicago, Illinois, USA.

⁸Department of Chemistry and Chemical Biology, Harvard University, Cambridge, Massachusetts, USA.

⁹These authors contributed equally to this work.

Abstract

New antibiotics with novel targets are greatly needed. Bacteria have numerous essential functions, but only a small fraction of such processes—primarily those involved in macromolecular synthesis—are inhibited by current drugs. Targeting metabolic enzymes has been the focus of recent interest, but effective inhibitors have been difficult to identify. We describe a synthetic azetidine

* hung@molbio.mgh.harvard.edu.

Author contributions

S.W. performed experiments with Mtb as well as kinetic and biophysical experiments with TrpAB. P.P.N. was responsible for chemistry. K.M., N.I.M., R.P.J., and A.J. were responsible for protein expression and purification, X-ray crystallography, and structure refinement and analysis. S.E.J. and B.B. developed and performed LC-MS analysis of kinetic assays. V.K.K. and S.W. performed calorimetry. N.S., A.E.C., S.C., and S.W. performed *in vivo* experiments. P.M. contributed to structural analysis and modeling. S.L.F., A.J., S.L.S., and D.T.H. advised on experiments and interpretation and together with S.W., K.M., and P.P.N. wrote the paper.

Competing financial interests

The authors declare no competing financial interests.

Additional information

Any supplementary information, chemical compound information and source data are available in the [online version of the paper](#). Reprints and permissions information is available online at <http://www.nature.com/reprints/index.html>. Publisher's note: Springer Nature remains neutral with regard to jurisdictional claims in published maps and institutional affiliations. Correspondence and requests for materials should be addressed to D.T.H.

derivative, BRD4592, that kills *Mycobacterium tuberculosis* (Mtb) through allosteric inhibition of tryptophan synthase (TrpAB), a previously untargeted, highly allosterically regulated enzyme. BRD4592 binds at the TrpAB α - β -subunit interface and affects multiple steps in the enzyme's overall reaction, resulting in inhibition not easily overcome by changes in metabolic environment. We show that TrpAB is required for the survival of Mtb and *Mycobacterium marinum in vivo* and that this requirement may be independent of an adaptive immune response. This work highlights the effectiveness of allosteric inhibition for targeting proteins that are naturally highly dynamic and that are essential *in vivo*, despite their apparent dispensability under *in vitro* conditions, and suggests a framework for the discovery of a next generation of allosteric inhibitors.

Mtb recently surpassed HIV as the world's leading cause of death due to infectious disease¹. The rise of multidrug resistance necessitates a deeper understanding of this complex bacterium to develop more efficient treatments with novel mechanisms of action²⁻⁴. Recent insight into Mtb biology has come with new agents, such as bedaquiline, which inhibits ATP synthase⁵, and delamanid, a nitroimidazole that inhibits mycolic acid synthesis and disrupts energy production^{6,7}. Despite such promising advances, many of the antitubercular compounds recently identified in whole-cell screening disproportionately hit cell wall targets⁸, including MmpL3 (ref. 9), DprE1 (ref. 10), FadD32 (ref. 11 and Pks13 (ref. 12). The excitement of uncovering different chemical scaffolds has, therefore, been dampened by the redundancy the targets and the failure to capitalize on the many other targets that should be available. This slow progress is perhaps a consequence both of the types of chemical libraries screened and of the screening methods.

We took advantage of a diversity-oriented synthetic (DOS) library that contains a rich stereochemical and skeletal variety compounds to perform whole-cell screening against wild-type (WT) Mtb. We identified a chiral azetidine derivative (2*R*,3*S*,4*R*)-3-(2'-fluoro-[1,1'-biphenyl]-4-yl)-4-(hydroxymethyl)azetidine-2-carbonitrile (BRD4592) (**1**), which has bactericidal activity exclusively in one of eight stereoisomeric forms. We found that BRD4592 allosterically inhibits Mtb TrpAB, an enzyme catalyzing the last two steps of L-tryptophan (L-Trp) biosynthesis¹³ (Fig. 1a).

TrpAB is encoded by *trpA* and *trpB*, which correspond to the α - and β -subunits of the functional $\alpha\beta\beta\alpha$ heterotetramer¹³. The α -subunits convert indole-3-glycerol phosphate (IGP) to indole and glyceraldehyde 3-phosphate (G3P), and the β -subunits, using pyridoxal 5'-phosphate (PLP) as a cofactor, catalyze the β -replacement reaction in which indole displaces the hydroxyl group of L-Ser to produce L-Trp¹³ (Fig. 1a and Supplementary Results, Supplementary Fig. 1). Studies of *Salmonella typhimurium* TrpAB have shown that indole is transferred from the α - to the β -subunit along a 25-Å hydrophobic channel¹³⁻¹⁵ to react with an L-Ser-PLP adduct¹⁶. Because L-Trp is the most energetically costly amino acid to produce^{17,18}, its biosynthesis is typically highly regulated at the transcriptional level and through allosteric control of enzyme activity¹⁷. Notably, the enzymatic activities and substrate channeling between the two active sites of TrpAB are coordinated by complex allosteric interactions between the subunits to optimize indole utilization^{13,19,20}, perhaps priming the enzyme for allosteric inhibition by xenobiotic small molecules.

Here we present a comprehensive report describing Mtb TrpAB and its inhibition by BRD4592. Through detailed kinetic, thermodynamic, and structural characterization, we find that BRD4592 is an allosteric, mixed-type inhibitor binding to a novel site in the channel between the enzyme's subunits. BRD4592 stabilizes active conformations of the enzyme complex, which have increased affinity for substrates and product, and stabilizes the interaction between the α - and β -subunits. The compound's multi-component mechanism is highly unique and results in inhibition that is not overcome by changes in the metabolic environment.

Because the essentiality of metabolic enzymes such as TrpAB often depends on the bacterial microenvironment, their indispensability must be confirmed *in vivo* to validate them as drug targets. We provide genetic evidence that TrpAB is required for the survival of Mtb in macrophages and mice and show that BRD4592 is effective in targeting TrpAB during mycobacterial infection of *Danio rerio* (zebrafish). Further, in contrast to a previous report²¹, our data suggest that Mtb L-Trp biosynthesis during *in vivo* infection is not dependent on T cells. These findings demonstrate the effectiveness of a strategy to target conditionally essential metabolic enzymes using allosteric small molecules and suggest general principles for allosteric probe discovery.

RESULTS

Discovery of an azetidine targeting tryptophan synthase

We screened the Broad Institute DOS library (82,762 compounds) synthesized using the build–couple–pair strategy²² against log-phase GFP-expressing Mtb⁸ (Supplementary Table 1). BRD4592 (Fig. 1b) had an *in vitro* MIC₉₀ (the minimal concentration needed to inhibit 90% of bacterial growth) of 3 μ M against Mtb. This azetidine contains three stereogenic centers, and only the BRD4592 stereoisomer was active, suggesting a high degree of target specificity. Similarly to bedaquiline, which has a delayed bactericidal response²³, BRD4592 reduced numbers of colony-forming units (CFUs) of Mtb cultures by 2–3 logs after several days of treatment (Fig. 1c). The compound had comparable activity against a diverse panel of Mtb clinical isolates, including drug-resistant strains (Supplementary Table 2), but had a 50% cytotoxicity concentration (CC₅₀) > 100 μ M against HepG2 human liver carcinoma cells and no activity in 36 screens reported in PubChem (compound ID 54650477).

To determine the mechanism of BRD4592 action, we selected for resistant Mtb mutants. Spontaneous mutants were obtained at a frequency of $\sim 8 \times 10^{-8}$, and each had an MIC₉₀ at least tenfold greater than that of the parent strain (Supplementary Table 2). All mutants contained point mutations in *trpA* (Rv1613), corresponding to alterations in amino acids α D136, α G66, or α P65, or *trpB* (Rv1612), corresponding to alterations in residue β N185 (Supplementary Table 2 and Supplementary Fig. 2a). Episomal expression of mutated *trpA*, but not WT *trpA*, was sufficient to confer resistance to BRD4592 in WT Mtb, showing that the resistant allele is dominant (Fig. 1d).

We tested BRD4592 against a panel of Gram-negative and Gram-positive bacterial species and found that it was active against several mycobacterial species but not other bacteria tested (Supplementary Fig. 2b). Notably, by sequence alignment, we found that α G66 is

conserved in all sensitive mycobacterial species but is altered in all naturally resistant non-mycobacterial species (Supplementary Fig. 2c). Given the observation that non-glycine substitutions at this position confer resistance to BRD4592 in Mtb (Supplementary Table 2), this substitution probably accounts for the intrinsic resistance of nonmycobacteria to BRD4592.

To complement the genetic data, we obtained metabolic evidence supporting TrpAB as the potential target of BRD4592. Addition of L-Trp to the growth medium rescued Mtb from the lethal effects of BRD4592 (Fig. 1d). Taken together, these data implicate TrpAB as the physiological target of BRD4592.

BRD4592 is an allosteric inhibitor of Mtb TrpAB

We next investigated the effect of the compound on recombinant Mtb TrpAB. To study the α -subunit reaction ($\text{IGP} \rightarrow \text{indole} + \text{G3P}$), we measured G3P production using a modified fluorescence-based assay²⁴. At L-Ser concentrations > 0.1 mM, the reaction is rate determining, and, therefore, the overall reaction can also be studied by this method. To follow the overall reaction ($\text{IGP} + \text{L-Ser} \rightarrow \text{G3P} + \text{L-Trp}$), we developed a complementary LC-MS method to separate and quantify indole and L-Trp simultaneously. We also used this assay to measure β -subunit activity exclusively ($\text{indole} + \text{L-Ser} \rightarrow \text{L-Trp}$).

We first characterized the kinetic mechanism of Mtb TrpAB to demonstrate that it is similar to previously characterized TrpAB complexes. We determined that apparent $K_M^{\text{L-Ser}} = 0.50 \pm 0.12$ mM and apparent $K_M^{\text{IGP}} = 32.6 \pm 8.1$ μM , with $k_{\text{cat}} = 19.6 \pm 3.9$ min^{-1} (Supplementary Fig. 3a,b)—similar values to those reported for *Escherichia coli* TrpAB²⁵. Reciprocal plots of velocity versus L-Ser and IGP concentration were linear (Supplementary Fig. 3c,d), indicating that Mtb TrpAB, like the *E. coli* enzyme, uses a double displacement mechanism, in which the reaction proceeds via two distinct half-reactions²⁵ with either IGP or L-Ser binding first²⁴.

We then investigated which steps of the TrpAB reaction are affected by BRD4592 and found that it potently inhibits both the α - and β -reactions; the IC_{50} for the α -subunit (IC_{50}^{α}) was 70.9 ± 7.0 nM, and the IC_{50}^{β} was 22.6 ± 11.5 nM (Fig. 2a,b and Supplementary Fig. 3e–g). TrpAB enzymes containing the amino acid substitutions αG66V and βN185S each showed a higher IC_{50}^{α} ($>1,000$ nM and 239.3 ± 3.1 nM, respectively), correlating with the higher whole-cell MIC_{90} of BRD4592 against Mtb harboring these mutant enzymes (Supplementary Fig. 4a,b). These data support the idea that inhibition of TrpAB is responsible for the activity of BRD4592 against whole Mtb cells.

That both steps of the reaction were affected suggests that BRD4592 does not simply inhibit one of the active sites. To further dissect our observations, we examined the relationship between BRD4592 and substrate binding. Under saturating IGP concentrations, BRD4592 was a mixed-type inhibitor versus L-Ser, with the apparent $K_i^{\text{L-Ser}} = 40.5 \pm 1.7$ nM and $\alpha = 0.81 \pm 0.06$ (Fig. 2c). The low α -value ($\alpha < 1$) indicates that TrpAB binds BRD4592 more tightly when L-Ser is also bound²⁵; isothermal calorimetry (ITC) confirmed this finding (Supplementary Fig. 5). We found that BRD4592 was uncompetitive versus IGP under saturating L-Ser concentrations, with apparent $K_i^{\text{IGP}} = 62.9 \pm 13.0$ nM (Fig. 2d). Together,

these data support a model in which BRD4592 is an allosteric inhibitor of both reactions and substrate binding to either subunit enhances TrpAB's affinity for the inhibitor.

To confirm that BRD4592 is an allosteric inhibitor of the α -reaction and distinct from direct inhibitors of the α -subunit active site, we compared BRD4592 to IGP substrate mimetics, including indole-propanol phosphate (IPP), F6, and F9 (refs. 19,26). Unlike BRD4592, these substrate mimetics were competitive with IGP²⁶ and were orders of magnitude less potent than BRD4592 against Mtb TrpAB (IPP, F6, and F9 $IC_{50}^{\alpha} = 255 \pm 41 \mu\text{M}$, $2.6 \pm 0.02 \text{ mM}$, and $1.3 \pm 0.08 \text{ mM}$, respectively; Supplementary Fig. 6a,c). Further, the α -subunit ligands had limited efficacy against the Mtb β -reaction (IPP $IC_{50}^{\beta} = 4.4 \pm 0.7 \text{ mM}$, Supplementary Fig. 6b,c). Finally, inhibition studies of TrpAB in combination with BRD4592 and IPP indicated that the enzyme was inhibited by the two compounds in an additive manner (Fig. 2e). Thus, BRD4592's mode of action is distinct from that of α -active site inhibitors.

BRD4592 stabilizes active states of the β -subunit

The α - and β -subunits interact extensively throughout the catalytic cycle, predominantly through the communication (COMM) domain¹³. Both subunits initially adopt an open, lowly active conformation ($\alpha^O\beta^O$)¹³. Upon L-Ser binding, this conformation is rapidly converted to an aminoacrylate intermediate state (E_{AA}), with the COMM domain of the β -subunit shifting into a closed, highly active state ($\alpha^O\beta^C$). Likewise, IGP substrate binding to the α -subunit promotes closing of the α -subunit (α^C) via movement of the $\alpha 16$ loop. Allosteric activation is mutual, with closing of the β -subunit triggering closing of the α -subunit and vice versa¹³. Both reactions and indole translocation occur with the enzyme in the closed state ($\alpha^C\beta^C$). Once catalysis is complete, the enzyme cycles back to the $\alpha^O\beta^O$ state (Supplementary Fig. 1).

Having shown that BRD4592 is an allosteric inhibitor of the α -reaction, we sought to understand BRD4592's mode of inhibition against the β -reaction. We used the absorbance spectrum of the β -subunit PLP cofactor to study the chemical state of cofactor–substrate adducts and, by inference, the conformational states of TrpAB¹⁹. As with *Salmonella* TrpAB¹⁹, Mtb TrpAB PLP absorbance spectra were consistent with a shift from a lowly active β^O conformation ($E_{A,Int}$) to a highly active β^C conformation (E_{AA}) upon L-Ser binding (Fig. 3a and Supplementary Fig. 1). Because this shift is associated with changes in absorbance that are dependent on L-Ser concentration¹⁹, we measured the apparent K_d^{L-Ser} in the presence and absence of BRD4592, with K_d values of $9.1 \pm 1.1 \mu\text{M}$ and $83.4 \pm 3.2 \mu\text{M}$, respectively (Fig. 3b). This result suggests, paradoxically, that though BRD4592 inhibits the β -reaction, it stabilizes the β^C conformation.

Using PLP absorbance, we found that BRD4592 also stabilizes two other closed forms of the β -subunit: one is bound to the indole analog indoline (2,3-dihydro-1H-indole) ($E_{Qindoline}$), and the other is bound to its product L-Trp (E_{Q3}) (Supplementary Fig. 7a,b). We also found that BRD4592 increases the affinity of TrpAB for L-Trp 4.5-fold (Supplementary Fig. 7c). These data showed that BRD4592 consistently shifts the conformational equilibrium toward chemical states associated with a closed, highly active β -subunit. Differential scanning calorimetry (DSC) confirmed these findings. In the absence of L-Ser, BRD4592 did not stabilize the open conformation (Fig. 3c); in contrast, in the presence of L-

Ser, BRD4592 binding increased the T_m of TrpAB in the active β^C conformation by 8 °C (Fig. 3d). Notably, BRD4592 also stabilized the enzyme complex against dissociation upon dilution (Supplementary Fig. 7d). Therefore, we concluded that BRD4592 specifically stabilizes closed states of the β -subunit.

Crystal structures reveal unique inhibitor binding site

To understand how BRD4592 interacts with the enzyme, we solved five crystal structures of Mtb TrpAB (Supplementary Tables 3 and 4), including an inhibitor-free, substrate-free form in the lowly active state ($\alpha^O\beta^O$), the aminoacrylate-bound form (E_{AA} ; $\alpha^O\beta^C$) (Fig. 3a), the BRD4592-bound form ($\alpha^O\beta^O$ -BRD4592), and the BRD4592-bound E_{AA} form ($\alpha^O\beta^C$ -BRD4592), as well as the α G66V mutant in the inhibitor-free, substrate-free form (α G66V β^O).

TrpAB is structurally heterogeneous and flexible. Although all crystals contained two $\alpha\beta\beta\alpha$ heterotetramers per asymmetric unit (chains A, C, E, and G correspond to α -subunits, and chains B, D, F, and H correspond to β -subunits), we observed substantial heterogeneity among the conformations of the β -subunits. In $\alpha^O\beta^O$ structures, the conformations of half of the β -subunits (chains D and F) were affected by crystal packing, which moved the COMM domain toward the protein core to adopt the β^O conformation most frequently observed in *Salmonella* TrpAB structures, whereas the other β -subunits (chains B and H), which were not constrained by neighboring molecules, adopted a more expanded open (β^{eO}) conformation (Supplementary Fig. 8a). This conformational heterogeneity was reflected in relatively high root-mean-square (r.m.s.) deviation values (0.58–0.61 Å) for superpositions of all C α atoms in β^{eO} and β^O chains.

Consistent with our finding that BRD4592 is an allosteric inhibitor, crystal structures showed that BRD4592 binds outside both active sites in a cavity located at the α – β interface (Fig. 3b,c). The observed conformational heterogeneity in $\alpha^O\beta^O$ structures affected BRD4592 binding, which adopts one well-ordered state in β^O (this state was used for further analysis below) and two somewhat different conformations in β^{eO} subunits. These subunits shifted toward the β^O state in BRD4592-bound structures, but this transition was not complete, and in chain H, two states were modeled, corresponding to β^{eO} (20% occupancy) and β^O (80%) conformations (Supplementary Fig. 9a,b).

The BRD4592 binding pocket intersects the hydrophobic tunnel through which indole presumably travels from the α – to the β -catalytic site (Fig. 3d,e). This novel and adaptable binding site is distinct from the recently reported *Salmonella* TrpAB intra-channel binding site of the F6 inhibitor observed at very high ligand concentrations²⁷ (Supplementary Fig. 8b). BRD4592 binding appears to be driven primarily through hydrophobic interactions between BRD4592 aromatic rings and β -subunit aromatic side chains, including β F188 and β F202, as well as β -subunit branch chain residues, including β I184 and β L34 (Fig. 3b). Direct and water-mediated hydrogen bonds connect the secondary amine and the hydroxyl groups of the azetidine ring with both subunits (α D64, α G66, and β H294) (Fig. 3b), further contributing to the stability of the enzyme–inhibitor complex and providing a clear explanation for the stereochemical requirements for binding. All altered amino acids identified in resistant Mtb mutants are clustered along the azetidine-binding site, and the

crystal structure of TrpAB with the α G66V mutation suggests that the α V66 isopropyl side chain sterically interferes with BRD4592 binding (Supplementary Fig. 9d).

To understand the impact of L-Ser on the enzyme–BRD4592 interaction, we compared the $\alpha^{\text{O}}\beta^{\text{O}}$ -BRD4592 structure without L-Ser with the $\alpha^{\text{O}}\beta^{\text{C}}$ -BRD4592 structure with L-Ser bound (E_{AA} state). In $\alpha^{\text{O}}\beta^{\text{C}}$ -BRD4592, the inhibitor molecule has more contacts with the protein than in the $\alpha^{\text{O}}\beta^{\text{O}}$ -BRD4592 conformation (67 versus 57) (Supplementary Fig. 9c). This is consistent with ITC data showing that BRD4592 binding to Mtb TrpAB is tighter in the presence of L-Ser (Supplementary Fig. 5).

We also found that BRD4592 binding affects the distribution of B factors around the inhibitor-binding site, seemingly reducing protein flexibility. Specifically, the α 12 loop, which contains the catalytic residue α D68 (ref. 28), showed lower isotropic B factors in the presence of BRD4592 (Supplementary Fig. 10a,b). A similar effect was observed for helix β h6, an α -subunit-facing section of the COMM domain that forms important activating interactions with the α -subunit²⁸ (Supplementary Fig. 10c–e). Multiple studies have established that the geometry of and the bonds formed by loops α 16 and α 12 have a pronounced effect on α -subunit activity^{29,30}, with changes in protein elements nearby preventing proper positioning of catalytic residue α D68 (ref. 28). Similar consequences could potentially result from reduced mobility of α 12 in the presence of BRD4592.

BRD4592 has a multifaceted mechanism of inhibition

Together, the biophysical and structural data revealed that BRD4592 is an allosteric inhibitor of both subunits, binding the α – β interface along the tunnel connecting the two. However, the data also pointed to a more complex mechanism of inhibition, as BRD4592 increases enzyme affinity for substrates and products, stabilizes subunit interactions, and shifts equilibrium toward closed, highly active conformations of the enzyme—all effects that are commonly associated with allosteric activators.

Our results showed that there are at least three components of TrpAB inhibition by BRD4592. First, indole production from IGP is prevented, probably because of reduced flexibility in the α 12 loop and β h6 helix, which may interfere with proper positioning of α -catalytic residues, and due to stabilization of the E_{AA} conformation of the β -subunit, which may prevent further progression through the catalytic cycle. Using high enzyme concentrations with IGP and L-Ser as substrates under saturating BRD4592 concentrations, we found that the α -reaction was initially slowed 245-fold ($k_{\text{cat}}^{\alpha} = 0.08 \pm 0.01 \text{ min}^{-1}$ versus $19.6 \pm 3.9 \text{ min}^{-1}$ with no BRD4592) (Supplementary Fig. 11c,d).

Second, BRD4592 also potently inhibits the β -reaction such that not all indole produced by the α -site reaction is converted to L-Trp (Supplementary Fig. 11e). At saturating BRD4592 concentrations and high enzyme concentrations, we were initially able to detect production of L-Trp from indole and L-Ser at a rate 750 times slower than the uninhibited enzyme ($k_{\text{cat}}^{\beta} = 0.26 \pm 0.01 \text{ min}^{-1}$ and $197 \pm 8.8 \text{ min}^{-1}$, respectively) (Supplementary Fig. 11a). BRD4592 stabilizes TrpAB bound to the indole analog indoline and is uncompetitive with respect to indole (Supplementary Figs. 7a and 3f), suggesting that BRD4592 may trap the enzyme in an indole-bound state, preventing catalytic cycling. Given the location of BRD4592, part of

the inhibition mechanism may also be to block the movement of indole through the tunnel, which is the substrate's main mode of entry into the β -active site^{14,31}. We presume the observed conversion of indole to L-Trp, albeit slow, may be due to entry of indole via an alternative, less accessible path or to slower entry via the tunnel. In contrast, the α -site ligands (IPP, F6, and F9) did not substantially inhibit the β -reaction ($k_{\text{cat}}^{\beta} = 42 \text{ min}^{-1}$ under 10 mM IPP, Supplementary Fig. 11b) though they also block the tunnel at higher concentrations³¹. It is possible that BRD4592 is simply more effective at blocking the tunnel or that BRD4592 inhibits the β -reaction through additional allosteric mechanisms.

Finally, we identified a third component to BRD4592's mechanism of inhibition. Under saturating BRD4592 concentrations, we observed time-dependent effect. Initially BRD4592 inhibited both the α - and β -reactions more than 200-fold, drastically reducing L-Trp production. However, after a small amount of L-Trp had been produced, the reaction stopped (Supplementary Fig. 11d,e). Addition of more IGP to this inhibited enzyme complex did not overcome the inhibition (Supplementary Fig. 11f). We determined that BRD4592 is a reversible inhibitor, and there was no evidence of slow binding or of the azetidine nitrile reacting covalently with TrpAB to explain the time-dependent inhibition (Supplementary Fig. 12). Instead, this final component may be due to product inhibition, as BRD4592 increases enzyme affinity for L-Trp and stabilizes closed conformations of the L-Trp-TrpAB complex (Supplementary Fig. 7b,c). Thus, any L-Trp produced by the inhibited enzyme may be trapped, preventing further catalytic cycling. By stabilizing multiple substrate- and product-bound states of TrpAB, BRD4592 achieves complete inhibition that cannot be overcome by addition of substrate and is strengthened by any product generated. The complexity of BRD4592's mechanism may be the basis for its high potency.

Mtb TrpAB is essential *in vivo*

BRD4592 is potent *in vitro*, and its inhibition is not overcome by increases in substrate concentration, making it an attractive inhibitor for *in vivo* applications. However, the ability to render the inhibitor ineffective against whole Mtb cells in environments with sufficient levels of L-Trp raised questions about TrpAB's essentiality under relevant *in vivo* conditions. Though other enzymes in the Mtb L-Trp biosynthetic pathway have previously been studied^{21,32}, the *in vivo* essentiality of Mtb TrpAB had not been assessed. A recent report suggested that Mtb can scavenge L-Trp from the host and further that CD4⁺ T cell-produced interferon- γ (IFN- γ) activates the host enzyme indoleamine 2,3-dioxygenase (IDO) to degrade host pools of L-Trp²¹. This work thus suggested that bacterial L-Trp biosynthesis essentiality is tied to an adaptive immune response.

We first studied the essentiality of TrpAB beyond axenic culture using BRD4592 in Mtb-infected macrophages. BRD4592 restricted Mtb growth in macrophages eight-fold compared to control treatment (DMSO; Fig. 5a). Next, we found that after 5 d of treatment, BRD4592 restricted *M. marinum* growth in zebrafish embryos by ~1.5 logs compared to DMSO control (Fig. 5b), demonstrating the *in vivo* requirement for TrpAB. Furthermore, when we infected zebrafish with a BRD4592-resistant strain of *M. marinum* harboring a mutation in *tpa* (MmTrpA^{G65S}; *M. marinum* $\alpha 65$ is equivalent to Mtb $\alpha 66$), we found that the mutant was not affected by BRD4592 treatment (Fig. 5b), demonstrating that the *in vivo* effect of

BRD4592 was on target. Notably, because the adaptive immune system has not yet matured in zebrafish at this early stage of development, this model has no T cells at the time of infection (2 d after fertilization (dpf); mature T cells leave the thymus at 6 dpf)^{33,34}.

Although we were unable to assess the efficacy of BRD4592 in mice owing to the pharmacokinetic properties of the molecule (mouse liver microsome intrinsic clearance (CL_{int}) = 336.2 $\mu\text{L}/\text{min}/\text{mg}$ and hepatocyte CL_{int} = 47.2 $\mu\text{L}/\text{min}/10^6$ cells; data not shown), we sought to confirm TrpAB essentiality in mammalian cells. We constructed a strain of Mtb with an in-frame clean deletion of *trpA* (H37Rv *trpA*). As expected, this strain required L-Trp for growth *in vitro* (Fig. 5c). Similarly to *trpE* deletions²¹, the *trpA* deletion mutant died much more rapidly than reported *trpD* knockout strains³². This could indicate differences in the accumulation of toxic intermediates in various L-Trp auxotrophs²¹, variable detection of and response to auxotrophy in these mutants, or varying metabolic burden resulting from unproductive progression through the L-Trp biosynthetic pathway. As expected, H37Rv *trpA* was also attenuated in macrophages^{21,32} (Fig. 5a). When H37Rv *trpA* was complemented with an episomal copy of *trpA* (H37Rv *trpA::trpA*), growth in the absence of supplemented L-Trp and survival in macrophages was restored (Fig. 5a,c).

To assess the essentiality of Mtb TrpAB in a mammalian host, we infected C57BL/6 mice with aerosolized H37Rv *trpA*, H37Rv *trpA::trpA*, or WT Mtb. Mice were sacrificed 24 h, 2 weeks, or 5 weeks after infection. Notably, at the 24-h time point, equal numbers of H37Rv *trpA* and WT Mtb were recovered (~50 CFU/mouse), confirming delivery of all strains to the lungs (Fig. 5d). The H37Rv *trpA* mutant was severely attenuated at later time points and was below the limit of detection in lung (45 CFU), spleen (45 CFU), and liver (90 CFU) at weeks 2 and 5 (Fig. 5d–f). In contrast, the WT and complemented strains grew to comparable levels (~50,000 CFU/lung) by week 2 and had disseminated to the liver and spleen by week 5 (Fig. 5d–f). As substantial adaptive immune responses in the lungs are not observed until after 2 weeks of infection in this well-characterized infection model³⁵, the inability to recover H37Rv *trpA* bacteria at 2 weeks suggests that TrpAB is likely to be essential independently of the CD4⁺ T cell-mediated IFN- γ response. Taken together, our findings demonstrate that L-Trp biosynthesis is required for mycobacteria during *in vivo* infection and that TrpAB inhibitors such as BRD4592 can be highly effective *in vivo*.

DISCUSSION

Significant effort is being invested in the discovery of new classes of antibacterial agents with novel mechanisms of action to counter the steady rise of resistance in bacteria. We have identified a novel azetidine, BRD4592, with a new molecular target in Mtb. Our data showed that BRD4592 binds at the protein–protein interface of TrpAB, revealing a new binding site in this well-studied enzyme. Paradoxically, despite a positive effect on enzyme stability and substrate affinity (hallmarks of allosteric activators), BRD4592 inhibits the activity of both subunits without substantially changing the structure of the active sites, thus probably mediating its effects from entropy-based changes in protein flexibility³⁶. We suggest that BRD4592 ultimately acts as an inhibitor via a combination of stabilizing crucial enzyme states and blocking indole shuttling between the two active sites, as well as stabilizing the

enzyme–product complex to prevent catalytic cycling. To our knowledge, this is the most complicated and multifactorial allosteric inhibitor reported for TrpAB to date, and for allosteric inhibitors in general.

Allosteric inhibition has great appeal for targeting metabolic enzymes, which typically have shallow active sites designed to accommodate polar, hydrophilic substrates—characteristics that conflict with drug-like properties required for both target engagement and permeation through cell membranes^{37,38}. Second, because of the relatively limited number of substrate entities that are recognized with high affinity, strategies to inhibit enzymes using substrate-like mimetics often result in compounds that have significant off-target effects^{39–41}. In contrast, BRD4592 is highly specific and is thus positioned as a useful probe for understanding the biology of L-Trp biosynthesis in Mtb, including the question of why starvation of some amino acids, including L-Trp, results in death for Mtb, whereas starvation of others results in a static response³². BRD4592 is also useful for exploring the requirement for L-Trp biosynthesis in mycobacteria throughout the course of an infection where the bacterium may encounter various environments.

Although targeting TrpAB is attractive, as the L-Trp biosynthetic pathway does not exist in humans, the questionable vulnerability of such metabolic processes *in vivo* has historically resulted in their dismissal as viable target candidates. Recently, however, conditional essentiality—the idea that the requirement for a gene or pathway is dependent on the specific physiological setting^{42,43,44}—has challenged the criteria for drug-discovery target validation and moved the field away from data based on rich or supplemented growth media to data based on minimal media and *in vivo* studies. Here, we showed BRD4592 is effective against Mtb in macrophages and *M. marinum* in zebrafish embryos and larvae and that H37Rv *tpaA* cannot survive infection in mice, validating its *in vivo* essentiality in models lacking T cells. Thus, we suggest that TrpAB essentiality can be independent of adaptive host immunity, which would be important in the setting of Mtb with HIV co-infection. Given recent work showing the importance of CD4⁺ T cell–produced IFN- γ in depleting host L-Trp and restricting Mtb growth²¹, we would expect TrpAB to be even more essential when coupled with the activity of the adaptive immune system. It is possible that IFN- γ produced by innate immune responses results in the requirement for L-Trp biosynthesis in earlier stages of infection, and we cannot fully rule out T cell involvement in our models. Nevertheless, these data demonstrate the requirement for TrpAB for survival during infection and the effectiveness of allosteric inhibition for targeting TrpAB during *in vivo* infection as a model for targeting central metabolic enzymes more generally.

There has been great interest in discovering allosteric inhibitors in many disease areas. Allosteric inhibitors often stabilize a specific conformation of their enzyme target to prevent catalytic cycling. For example, a recent allosteric inhibitor of SHP2 functions by stabilizing the enzyme's inactive conformation⁴⁰. In contrast, BRD4592 stabilizes multiple conformational states, resulting in inhibition that cannot be easily overcome by changes in metabolic environment and is, in fact, enhanced by increases in substrate or product concentration. The extreme rarity of uncompetitive inhibitors has been previously highlighted, and uncompetitive inhibitors of metabolic enzymes have been suggested to be potentially more effective than competitive inhibitors⁴⁵. This is due to substantially greater

increases in intermediate concentrations as a result of uncompetitive inhibition and the inability of these high substrate concentrations to overcome uncompetitive inhibition. Indeed, BRD4592 clearly demonstrates this principle. Given how diverse the host niche for Mtb can be and that the environment can fluctuate with regard to abundance of various nutrients and metabolites, it is very important for any antitubercular compound targeting central metabolism to be active in a variety of metabolic environments. As such, BRD4592 may represent a prototype of next-generation allosteric inhibitors, developed for their complex mechanisms that result in increased potency and provide robust inhibition in the face of changing environmental conditions.

Finally, our findings suggest that highly dynamic, multi-subunit enzymes with natural allosteric regulation provide prime targets for such allosteric inhibitors. The heterogeneity observed in our collection of Mtb TrpAB crystal structures provides definitive evidence of conformational flexibility in this system, consistent with flexibility reported in other TrpAB enzymes^{15,16,28}. Such flexibility is considered a critical feature of allosteric proteins, necessary for the communication of signals across protein subunits³⁶, which must tailor enzyme activity rapidly in response to changing environments. Here we suggest that the different conformations required by the TrpAB complex throughout its catalytic cycle provide ample opportunity for small molecules to bind and destabilize or, in this case, stabilize certain enzyme states and reduce protein flexibility to prevent catalytic cycling. The complex inhibitory mechanism of BRD4592 indicates that the sensitivity of TrpAB's activity to different conformations makes it particularly vulnerable to inhibitors that can bind and disrupt the transmission of allosteric signals within the enzyme. In addition, this work suggests that understanding the relationships between inhibitor, substrate and product binding are important aspects of probe discovery, both for the development of more potent inhibitors and for understanding enzyme dynamics and the various ways in which the enzyme's microenvironment could affect probe activity. The adoption of routine assessment of substrate and product interactions will, therefore, be important for the identification and development of allosteric inhibitors. For screening campaigns designed to identify novel allosteric inhibitors, a thorough characterization of confirmed hits with respect to altered affinities of substrates or products can potentially inform the rational prioritization of scaffolds. Thus, our discovery of a unique and complex inhibitor suggests general principles that may lead to new, highly potent allosteric inhibitors.

METHODS

Methods, including statements of data availability and any associated accession codes and references, are available in the [online version of the paper](#).

ONLINE METHODS

High-throughput screening.

The Broad Institute's synthetic Diversity Oriented Synthesis (DOS) library (82,762 compounds) was screened against Mtb as previously reported⁸ (Supplementary Table 1). Briefly, replicating Mtb ($OD_{600} = 0.6-0.8$) constitutively expressing GFP was incubated with 25 μ M compound (dissolved in DMSO), rifampicin (positive control), or DMSO

(negative control) in 384-well plates for 3 d, at which time GFP fluorescence was read using a SpectraMax M5 (Molecular Devices). *Z*-scores were determined per plate.

Chemistry.

All reagents and solvents other than BRD4592 were obtained from commercial sources and used without further purification. BRD4592 was synthesized and purity confirmed as described in the Supplementary Note. For use in assays, BRD4592 was dissolved in DMSO.

All oxygen- and/or moisture-sensitive reactions were carried out under N₂ atmosphere in glassware that had been flame-dried under vacuum (0.5 mm Hg) and purged with N₂ before use. NMR spectra were recorded on a Bruker 400 (400 MHz ¹H, 101 MHz ¹³C) or Varian (400 MHz ¹H, 101 MHz ¹³C) spectrometer. All chemical shifts are reported in parts per million (δ) with tetramethylsilane as an internal standard. Data are reported as follows: chemical shifts, multiplicity (br, broad; s, singlet; d, doublet; t, triplet; q, quartet; dd, doublets of doublet; m, multiplet; coupling constant(s) (*J* values) in Hz; integration). Unless otherwise indicated, NMR data were collected at 25 °C. Flash chromatography was performed using 100–200 mesh silica gel with the indicated solvent. LC-MS analysis was performed on a LC-20AB/AD separations module (Shimadzu) or a 1200 Series (Agilent), operating in ESI (+ or –) ionization mode. Analytes were eluted using a linear gradient of 0.037% TFA + H₂O (V/V), 0.018% TFA + CH₃CN (V/V) or 10 mM NH₄HCO₃ containing H₂O + CH₃CN mobile phase. Preparative HPLC was performed on a 281 separations module (Gilson, Inc.) or LC-8A separations module (Shimadzu); MS spectra were recorded using a 3100 Mass Spectrometer (Waters) with electrospray ionization. Samples were eluted using a linear gradient of 0.1% TFA in H₂O + CH₃CN or 0.04% HCl in H₂O + CH₃CN or 0.2% formic acid in H₂O + CH₃CN, or 10 mM NH₄HCO₃ in H₂O + CH₃CN, or 0.04% NH₄OH in H₂O + CH₃CN. Analytical thin layer chromatography (TLC) was performed on 0.2-mm silica gel plates. Visualization was accomplished with UV light and aqueous potassium permanganate (KMnO₄) stain followed by heating.

Mtb strains and growth conditions.

M. tuberculosis (Mtb) H37Rv was used for all experiments unless otherwise noted. Mtb was grown at 37 °C in Middlebrook 7H9 supplemented with 10% oleic albumin dextrose catalase (OADC) and 0.05% Tween-80 and 0.05% glycerol or on Middlebrook 7H10 plates supplemented with 10% OADC and 0.2% glycerol. H37Rv *trpA* was grown in the same medium supplemented with 1 mM L-Trp. The plasmid pUV3583c was used to constitutively overexpress *trpA* in WT H37Rv and H37Rv *trpA::trpA*.

Determination of dose-response curves and MIC₉₀s.

Bacteria were grown to mid-log phase, then added to 96-well plates at OD₆₀₀ = 0.025 and grown in the presence varying BRD4592 concentrations for 2 weeks. Growth was assessed by OD₆₀₀. The minimal inhibitory concentration, MIC₉₀, was defined as the minimum concentration that inhibited growth by 90% relative to a DMSO control.

For growth curves, Mtb was grown to mid-log phase and diluted to $OD_{600} = 0.0025$ in inkwells containing the indicated amounts of BRD4592 in triplicate. Aliquots were plated to determine colony-forming units (CFU) at the time points indicated.

Generation of resistant mutants.

The agar MIC of BRD4592 was determined by plating bacteria on agar containing a dose response of compound in a 96-well format. Resistant mutants were generated by plating 1×10^9 bacteria on agar containing 2 \times , 4 \times , and 10 \times the agar MIC using four independently derived wild-type clones of H37Rv Mtb. Four independent parent clones were used in order to avoid the selection of drug-resistant siblings. Colonies were inoculated into liquid medium containing 6 μ M BRD4592. These cultures were retested in a liquid MIC assay to confirm resistance and used to generate genomic DNA for whole genome sequencing.

Mtb *trpAB* gene cloning.

The *trpB-trpA* operon was amplified from Mtb H37Rv genomic DNA using primers 5' - GGAGTAAAGATAATGAGTGCTGCCATCGCCGAAC and 5' - GTGATGGTGATGATGTGCGGACATCCCTAGTCGTACC using KOD HOT START polymerase in the presence of 2.5 M monohydrate betaine. The PCR product was purified and treated with T4 polymerase in the presence of dGTP according to previously published methods⁴⁶ followed by ligation independent cloning (LIC) to pMCSG81 (ref. 47 and <http://dnasu.org/DNASU/GetVectorDetail.do?vectorid=661>). Vector pMCSG81 expresses proteins with the non-cleavable C-terminal His₆ tag. The expression of Mtb TrpB from the polycistronic operon was satisfactory, but Mtb TrpA expression was low. Altering the ribosome-binding site (rbs) upstream of the *trpA* gene improved expression level. Polymerase Incomplete Primer Extension (PIPE) cloning was performed as described previously⁴⁸ using primers 5' - GTTAACTTTAAGAAGGAGATATACATATGGTGGCGGTGGAACAGAGC and 5' - CTCCTTCTTAAAGTTAAACACCATTTTCAGTCGTTGCCAGCAAGCCAAAC to generate MtbTrpB-MtbTrpA-pMCSG81 plasmid. To further increase the expression of the TrpA subunit, the *trpA* gene alone was inserted using LIC into vector pMCSG81-pRSF with resistance to kanamycin and the RSF origin of replication (primers 5' - GGAGTAAAGATAATGGTGGCGGTGGAACAGAGC and 5' - GTGATGGTGATGATGTGCGGACATCCCTAGTCGTACC). The resulting plasmid was named MtbTrpA-pMCSG81-pRSF. For production of stable Mtb TrpAB complex *E. coli* BL21-Gold (DE3) was co-transformed with both vectors.

α G66V and β N185S mutant gene cloning.

PIPE cloning procedure was performed on plasmids MtbTrpB-MtbTrpA-pMCSG81 and MtbTrpA-pMCSG81-pRSF. Primers 5' - GGACCCGGTCATGGACGGCCCCACCAT and 5' - CGTCCATG|ACCGGGTCCGAATACGGAAC were used for amplification resulting in Mtb TrpB-MtbTrpA(G66V)-pMCSG81 and MtbTrpA(G66V)-pMCSG81-pRSF. An identical procedure was performed to create MtbTrpB(N185S)-MtbTrpA-pMCSG81 using primers 5' - GACGCCATCAGTGAGGCGTTCCGGGATTGGGTT and 5' - GAACGCCTCACTGATGGCGTCTTTGAGCGTTTTTCGA.

Mtb TrpAB expression.

MtbTrpB-MtbTrpA-pMCSG81 and MtbTrpA-pMCSG81-pRSF were co-transformed to *E. coli* BL21-Gold (DE3) and selected against ampicillin (150 µg/mL) and kanamycin (30 µg/mL) in LB medium supplemented with 40 mM K₂HPO₄ and 2 g glucose per liter (LB-PO₄-glucose medium). A starter culture was grown overnight at 37 °C on a shaker set to 200 r.p.m. The following morning, 12 L of LB-PO₄-glucose medium with antibiotics was inoculated with overnight culture. After reaching OD₆₀₀ of 1.0, the culture was cooled to 20 °C and supplemented with 50 µM pyridoxal 5'-phosphate (PLP), and protein expression was induced with 0.3 mM IPTG. The growth was continued for another 20 h at 20 °C at 190 r.p.m. An additional 6 L LB medium culture with only MtbTrpA-pMCSG81-pRSF was grown under the same conditions. Finally, cells harvested from 12 L MtbTrpB-MtbTrpA-pMCSG81 and 6 L MtbTrpA-pMCSG81-pRSF were suspended in buffer A (50 mM HEPES:NaOH, pH 7.5; 150 mM KCl; 20 mM imidazole, pH 8.0; 5% glycerol; 1 mM TCEP; 1 mM PLP; 1 mM L-Ser). The cell suspension was frozen and stored at -80 °C. αG66V and βN185S mutants were overexpressed in the same conditions using appropriate plasmid combination.

Mtb TrpAB purification.

Frozen cells were thawed and sonicated (5 min total time, 130 W power output) and spun at 30,000 × *g* at 4 °C for 1 h. The initial Ni²⁺ affinity purification step was performed using a 2.5-cm × 10-cm Flex-Column connected to a Van-Man vacuum manifold (Promega). Supernatant was loaded on 5 mL Ni²⁺ Sepharose (GE Healthcare Life Sciences) equilibrated with buffer A and mixed thoroughly with the resin. Vacuum of 15 p.s.i. was used to speed removal of supernatant as well as wash out of unbound proteins (200 mL buffer A). The TrpAB complex was eluted with 25 mL buffer A supplemented with 500 mM imidazole, pH 8.0. The eluate was concentrated to about 2 mL and loaded on a Superdex 200 16/70 size exclusion column (GE Healthcare Life Sciences) equilibrated with buffer A. Successful crystallization required the presence of two protein peaks, one containing the TrpAB complex and another containing excess of the TrpA subunit. Fractions containing the TrpAB complex were collected, and buffer A was replaced with crystallization buffer (20 mM HEPES:NaOH, pH 7.5, 150 mM KCl; 1 mM PLP, 1 mM L-Ser, 1 mM TCEP) on Amicon 100-kDa-cutoff concentrators (Millipore). The TrpAB complex was concentrated to ~36 mg/mL. The same procedure was applied to αG66V and βN185S mutant purification. During purification, sample exposure to light was reduced as much as feasible.

Mtb TrpAB *in vitro* kinetic assays.

Prior to use, cryoprotected, purified protein was dialyzed against buffer containing 20 mM HEPES (pH 8.0), 100 mM KCl, 40 µM PLP, and 0.5 mM TCEP (TrpAB buffer). For most kinetic assays, 100 nM TrpAB was used. IC₅₀ against the β reaction was determined using 50 nM TrpAB and rates under saturating BRD4592 concentrations (Supplementary Fig. 11) were determined using 500 nM TrpAB. TrpAB concentration was calculated on the basis of the weight of the TrpAB dimer.

In the fluorescence-based assay, TrpAB was prepared in TrpAB buffer with 0.5 mM GAPDH, 2.5 mM NAD⁺, and 0.015 M sodium pyrophosphate (pH 8.5) with 0.03 M sodium

arsenate²⁴. Substrates were added to the wells of a black 96-well plate with a clear, flat bottom, and enzyme in buffer was added to start the reaction. Reaction progress was monitored by NADH fluorescence (excitation 340 nm, emission 460 nm). BRD4592 was not found to inhibit GAPDH activity in these conditions.

In the liquid chromatography–mass spectrometry (LC-MS) based assay, TrpAB was prepared in TrpAB buffer. After 5–10 min incubation (linear range of reactions was pre-determined by monitoring the reaction via absorbance at 290 nm), reactions were quenched using 3 volumes 0.1% formic acid in methanol followed by storage at 4 °C for 2 h. Samples were then centrifuged, and an aliquot of the supernatant was diluted 1:1 with water. 3.75 μ L of the final solution was injected. L-Trp and indole were detected by UPLC-MS (Waters). Compounds were quantified by selected ion recording (SIR) on a SQ mass spectrometer by negative electrospray ionization. The SIR method was set for L-Trp at 203.4 m/z and for indole at 116.3 m/z . Mobile phase A consisted of 0.1% ammonium hydroxide in water, while mobile phase B consisted of 0.1% ammonium hydroxide in acetonitrile. The gradient ran from 2% to 95% mobile phase B over 2.65 min at 0.9 mL/min. A BEH C18, 1.7- μ m 2.1-mm \times 50-mm column (Acquity) was used with column temperature maintained at 65 °C.

V_{\max} , K_M , and k_{cat} values were determined using nonlinear fitting based on Michaelis-Menten kinetics in GraphPad Prism. IC_{50} values were determined under balanced conditions (substrate concentration = K_M). BRD4592 inhibition data were analyzed using nonlinear enzyme inhibition equations in GraphPad Prism. For BRD4592 versus L-Ser (with saturating IGP concentration), a mixed-type inhibition model fit the data best ($R^2 = 0.9841$) whereas for BRD4592 versus IGP (with saturating L-Ser concentrations), mixed and uncompetitive inhibition models fit equally well ($R^2 = 0.9883$). The lines in a double reciprocal plot of 1/rate versus 1/IGP concentration (Fig. 2d) are nearly parallel and using this analysis method, α values are < 0.00001 , making BRD4592 effectively uncompetitive versus IGP.

Static UV–visible absorbance spectra.

Static UV-visible (UV-vis) absorbance spectra were measured on a Cary 4000 UV-Vis (Agilent Technologies). L-Ser was titrated into Mtb TrpAB (15 μ M) in TrpAB buffer without added PLP, with or without BRD4592 (200 μ M), and the absorbance spectrum at 350–550 nm was collected. Binding of L-Ser to Mtb TrpAB was followed by changes in the absorbance at 412 nm, corresponding to the disappearance of the substrate-free species. Titration plots were fit to a hyperbolic equation¹⁹ (1) to calculate K_d superior. For L-Trp binding, the same experimental conditions were used, except binding was calculated based upon changing absorbance at 475 nm⁴⁹.

$$\Delta A = (A_{\infty} - A_0)[L - \text{Ser}] / (K_d^{\text{apparent, L-Ser}} + [L - \text{Ser}]) \quad (1)$$

To assess the effect of indoline (2,3-dihydro-1H-indole) on the absorbance spectrum, 30 mM indoline was added to 15 μ M Mtb TrpAB with 20 mM L-Ser in TrpAB buffer without PLP, and the absorbance spectrum at 350–550 nm was collected. 200 μ M BRD4592 was added and the absorbance spectrum was measured again.

Differential scanning calorimetry (DSC).

Mtb TrpAB (0.5 mg/mL) was diluted in TrpAB buffer and melted using a Microcal VP Capillary DSC (GE Healthcare Life Sciences). Data were collected at 20–110 °C, with a 200 °C/h scan rate and 8-s filtering period. Data were analyzed in Origin software. For experiments involving L-Ser, TrpAB was incubated with L-Ser for at least 2 h before melting.

Crystallization and ligand soaking.

Crystallization experiments were conducted using the sitting-drop vapor-diffusion method with the help of the Mosquito liquid dispenser (TTP LabTech) in 96-well CrystalQuick plates (Greiner Bio-One), where 0.4 μ L protein solution at 20 mg/ml and 0.4 μ L crystallization solution were mixed, and the mixture was equilibrated against 135 μ L corresponding well solution. Trials were performed at 4 °C and 16 °C using several protein-to-reservoir ratios (2:1, 1:1, 1:2) and commercially available screens. Crystals usually appeared the next day and continued growing and forming over time. The crystals suitable for structure determination appeared in 5–90 d. Tests showed that some crystals contained the Mtb TrpB protein only. The best crystals of the Mtb TrpAB complex appeared at 16 °C in the PEG/Ion/F6 condition (8% v/v tacsimate, pH 8.0, 20% w/v PEG 3350) (Hampton Research) but initially diffracted to 4 Å only. Crystallization from the PEG/Ion/F6 condition was optimized by altering pH, precipitant concentrations and using two additive screens (Hampton Research and Jena Bioscience). Ultimately, the additive screen from Hampton at 16 °C and 2:1 protein-to-reservoir ratio produced robust diffraction-quality crystals, which were also suitable for inhibitor soaking. Further improvement of the purification protocol also enabled obtainment of better-quality crystals in the original screen condition. Crystallization plates were kept in the dark.

Crystals of the Mtb TrpAB complex in the open conformation ($\alpha^0\beta^O$) were obtained from PEG/Ion/F6 with additive B4 (8% v/v tacsimate, pH 8.0, 20% w/v PEG3350, 0.1 M KCl). For data collection at 100 K, the crystals were cryoprotected with mother liquor supplemented with 17% (v/v) ethylene glycol. The structure in the closed conformation ($\alpha^0\beta^C$) was obtained from crystals grown with additive G1 (8% v/v tacsimate, pH 8.0, 20% w/v PEG3350, 3% w/v trimethylamine *N*-oxide dihydrate) and soaked for 3–5 min in the mother liquor with 80 mM CsCl, 30 mM L-Ser, and 17% (v/v) ethylene glycol for cryoprotection.

The structure of the TrpAB complex with BRD4592 in the open conformation ($\alpha^0\beta^O$ -BRD4592) was obtained from crystals from the initial condition PEG/Ion/F6 which were soaked with 10 mM BRD4592 and 15% v/v ethylene glycol for 2–3 min. For the $\alpha^0\beta^C$ -BRD4592 structure in closed conformation, the TrpAB complex was co-crystallized with the BRD4592 inhibitor in PEG/Ion/F6 conditions with additive A1 (8% v/v tacsimate, pH 8.0, 20% w/v PEG3350, 10 mM BaCl₂, 1 mM BRD4592) and crystal was soaked with 100 mM CsCl and 50 mM L-Ser for 2–3 min followed by cryoprotection with 16% (v/v) ethylene glycol.

The structure of the α G66V mutant in the open conformation (α G66V β^O) was obtained from crystals grown in the original condition PEG/Ion/F6 and cryoprotected with 20% v/v ethylene glycol.

Data collection.

Prior to data collection at 100 K, all cryoprotected crystals were flash-cooled in liquid nitrogen. All X-ray diffraction experiments were carried out at the Structural Biology Center 19-ID beamline at the Advanced Photon Source, Argonne National Laboratory. The diffraction images for $\alpha^O\beta^O$, $\alpha^O\beta^O$ -BRD4592, $\alpha^O\beta^C$ -BRD4592, and α G66V β^O were recorded on the ADSC Q315r detector, and those for $\alpha^O\beta^C$ were recorded on the Pilatus3 6M detector. The data sets were processed with the HKL3000 suite⁵⁰. Intensities were converted to structure factor amplitudes in the Ctruncate program^{51,52} from the CCP4 package⁵³. The data collection and processing statistics are given in Supplementary Table 3.

Structure solution and refinement.

The $\alpha^O\beta^O$ structure was solved by molecular replacement in Phaser⁵⁴ with the *Salmonella enterica* homolog (PDB 1KFJ) as a search template. Following autobuilding in PHENIX⁵⁵, the final model was obtained through alternating manual rebuilding in COOT⁵⁶ and maximum-likelihood refinement in PHENIX and Refmac^{53,57}. Similarly, the subsequent structures were manually corrected in real space and crystallographically refined in Refmac. The refinement protocol included optimization of TLS parameters with one group per protein chain. The refinement statistics are shown in Supplementary Table 3. The details of asymmetric unit contents are provided in Supplementary Table 4. For these structures, 98.1%, 97.9%, 97.7%, 97.9%, and 98.1% of residues fall into favored regions of the Ramachandran plot, with 3, 4, 4, 4, and 3 residues being outliers, respectively.

Structure analysis.

Given the conformational heterogeneity observed in TrpAB structures, structural analysis of $\alpha^O\beta^O$ -BRD4592 was based primarily on the well-ordered chains C (α -subunit) and D (β -subunit). Superpositions were performed using the SSM algorithm, as implemented in CCP4 (ref. 53). For analysis of atomic displacement parameters, a separate refinement run in Refmac was performed with no TLS. The resulting model was used for further calculations in PHENIX⁵⁵. Cavity volumes were calculated in SPACEBALL⁵⁸, with probe radius of 1.42 Å, grid size of 0.3 Å in all directions, and one rotation. Alternative conformations were removed for calculations. Analysis of contacts between BRD4592 and the protein was performed in UCSF Chimera with default parameters⁵⁹. Structural figures were prepared in UCSF Chimera and The PyMOL Molecular Graphics System version 1.6 (Schrödinger, LLC).

H37Rv *trpA* construction.

In the Mtb tryptophan biosynthesis operon, *trpA* overlaps *trpB* upstream and *lgt* downstream by a single nucleotide. The *trpA* deletion strain was constructed by replacing the native operon with *trpB* engineered to overlap *lgt* in the same manner that *trpA* overlaps each gene. Gibson assembly was used to stitch together *trpB* and *lgt* into the suicide vector pJG1100.

The plasmid was transformed into Mtb and selected for using hygromycin (50 µg/mL) and kanamycin (15 µg/mL), then counter-selected by plating on sucrose. The resulting clones were picked into liquid medium and spotted on 7H10 with or without L-Trp, hygromycin, or kanamycin. Clones that grew only on 7H10 supplemented with L-Trp were expanded. PCR of the region around *trpA* followed by Sanger sequencing confirmed the clean deletion of *trpA*. The deletion strain was complemented with pUV3583c constitutively expressing *trpA*. All media used for deletion strain construction contained 1 mM L-Trp.

Macrophage infection model.

Wild-type Mtb H37Rv, H37Rv *trpA*, or its complement (H37Rv *trpA::trpA*) were used to infect J774 macrophages (ATCC). Mtb was added to macrophages at a multiplicity of infection of 1 and incubated for 4 h, at which point extracellular bacteria were washed away and fresh medium with or without drug was added to the wells containing macrophages. Infections were incubated 3 d, then macrophages were lysed with Triton X-100 (0.5%), and surviving bacteria were enumerated by CFU. Cell lines were verified to be free of mycoplasma contamination using the ATCC universal mycoplasma detection kit.

Mouse infections.

Female C57BL/6 mice were obtained from Jackson Laboratory. Mice were infected with 10⁵ CFU/mL aerosolized WT Mtb H37Rv, H37Rv *trpA*, or H37Rv *trpA::trpA*. At 24 h after infection, 3 mice per group were sacrificed, and lungs were harvested and plated for CFU. At 14 d and 35 d after infection, 5 mice per group were sacrificed, and lung, liver, and spleen were harvested and plated for CFU. The protocols, personnel, and animals used were approved and monitored by the Institutional Animal Care and Use Committee of the Harvard T.H. Chan School of Public Health. The animal facilities are AALAC accredited. Sample sizes were selected using SSCohort (OpenEpi, version 3) with the following parameters: 1-alpha = 95, 1-beta = 80, unexposed/exposed = 1, percent of unexposed with outcome = 0.1, percent of exposed with outcome = 99.

Zebrafish infections.

BRD4592-resistant *M. marinum* colonies were isolated from wild-type *M. marinum* carrying pUV3583c-gfp, a plasmid with GFP expression and kanamycin resistance. Single-cell suspensions of *M. marinum* were prepared for infection by washing log-phase bacteria twice in PBS + Tween-80 (0.05%), sonicating in a B2500A-MT water-bath sonicator (VWR Scientific) for five 1-min cycles with 30 s between cycles. Cultures were then pelleted and resuspended 50-fold concentrated. The concentrated culture was centrifuged at 500 r.p.m. for 5 min to remove large clumps of bacteria. The supernatant was filtered through a 5-µm filter to isolate single bacteria. Optical density of the final culture was measured and cultures were diluted or concentrated to a final concentration of ~300 CFU/nL. Aliquots of the single-cell preparation were frozen at -80 °C and thawed immediately before infection. Zebrafish embryos to be used for infections were treated with bleach (~0.005%) 24 h after fertilization (hpf) to minimize contamination of embryos with non-mycobacterial species derived from the fish facility before infection⁶⁰.

Embryos at 48 hpf were inoculated intravenously with ~500 CFU *M. marinum* in the duct of Cuvier¹¹. Infected embryos were treated with DMSO or BRD4592 for 5 d, then euthanized, washed once in PBS, and homogenized in 0.1% Triton X-100 with 5-mm stainless steel beads in three 2-min cycles of 40 Hz using a TissueLyser bead mill (Qiagen). Homogenates were vortexed well between bead mill cycles and just before plating on 7H10 agar supplemented with 15 µg/ml kanamycin to enumerate colonizing *M. marinum*. For all whole-organism studies, no blinding or randomization was used.

Metabolic stability assays.

Mouse liver microsomes (0.5 mg/mL) or hepatocytes were incubated with NADPH and BRD4592 (1 µM) for 0, 5, 10, 20, 30, and 60 min. Remaining compound concentration was determined using LC-MS/MS.

Additional bacterial strains and growth conditions.

The following strains were used in addition to Mtb: *M. marinum*, *M. smegmatis* (mc²155), *M. goodii* (ATCC #14470), *M. intracellulare* (ATCC #13950), *M. kansasii* (ATCC #12478), *M. abscessus* (ATCC #19977), *M. fortuitum* (ATCC #6841), *Salmonella typhimurium* (SL1344), *Pseudomonas aeruginosa* (PA01), *Staphylococcus aureus* Newman, *Vibrio cholerae* (O395 and C6706), *V. cholera* O395 *tolC*, *E. coli* (K12), and *E. coli tolC*. *M. smegmatis* was grown in Middlebrook 7H9 supplemented with albumin, dextrose, and saline (ADS). All other mycobacteria were grown in 7H9 supplemented with 10% OADC, 0.2% glycerol and 0.05% Tween-80. *S. typhimurium* was grown in Mueller–Hinton Broth and in N-minimal media. All other strains were grown in LB, M9 minimal medium, and M9 medium supplemented with casamino acids. Activity of BRD4592 was tested in both rich and minimal medium. *M. marinum* was grown in the dark at 30 °C, and all other bacteria were grown at 37 °C.

TrpA sequences and alignment.

FASTA sequences for TrpA from each bacteria were downloaded from UniProt and aligned using the multiple sequence alignment tool Clustal Omega from EMBL-EBI.

Isothermal calorimetry.

Isothermal calorimetry was performed using a MicroCal Auto-iTC200 (Malvern Instruments Ltd). 250 µM BRD4592 was injected into a cell containing 45 µM Mtb TrpAB in TrpAB buffer. Buffer, DMSO, and L-Ser concentrations were matched between the syringe (containing the compound) and the cell (containing the protein) to ensure that all observed effects were due only to the compound. BRD4592 was added in 40 injections of 1 µL at 25 °C with reference power set to 10 µCal/s. Results were analyzed using Origin software.

ANS binding assay.

8-anilino-1-naphthalene sulfonic acid (ANS) (20 µM) was incubated in a quartz cuvette with Mtb TrpAB (10 µM) in TrpAB buffer with or without L-Ser (20 mM) and without added PLP. To ensure ANS and TrpAB concentrations remained constant, concentrated BRD4592 was prepared in TrpAB buffer with ANS (20 µM) and TrpAB (10 µM) with or without L-Ser

(20 mM) and titrated into the cuvette. The fluorescence spectrum of ANS was measured using a SpectraMax M5 to excite at 380 nm and read emission at 400–600 nm. The change in fluorescence emission at 480 nm was used to calculate the K_d^{apparent} of BRD4592 by fitting to a hyperbolic equation (equation (2))¹⁹.

$$\Delta F = (F_i - F_n)[\text{BRD4592}] / (K_d^{\text{apparent}} + [\text{BRD4592}]) \quad (2)$$

Jump dilutions.

TrpAB (1 μM) in buffer with or without L-Ser was incubated with or without BRD4592 (1.5 μM) for 30 min at room temperature. The mixture was diluted 100-fold with buffer containing IGP for a final reaction mixture with 10 nM TrpAB, 0.5 mM L-Ser, 30 μM IGP, and 15 nM BRD4592. The reaction was incubated for 60 min to allow production of measurable levels of L-Trp and activity was measured using LC-MS detection of L-Trp. As a control, TrpAB that was not pretreated with BRD4592 was treated with BRD4592 upon addition of IGP to start the reaction.

Liquid chromatography–mass spectrometry (LC-MS).

Mtb TrpAB (0.2 mg/mL) was incubated with BRD4592 (250 μM) or DMSO for 2–3 h at room temperature. The mass of intact TrpAB protein was determined using LC-ESI-MS (QExactive; ThermoFisher). Briefly, 10 μL protein (0.1 mg/mL) was injected onto a 3.5- μm 2.1 \times 100 mm Zorbax 300SB-C8 column (Agilent Technologies) in 85% aqueous (0.1% formic acid in water) and 15% organic (0.1% formic acid in acetonitrile) phases. The protein was eluted using a linear gradient from 15% to 75% organic phase over 10 min. The mass spectrometer settings were as follows: positive mode, full-MS scan range (800–2,100 m/z); resolution, 70,000; AGC target, 3×10^6 ; maximum inject time, 200 ms; microscans, 3; sheath gas flow rate, 35; auxiliary gas flow rate, 5; sweep gas flow rate, 0; spray voltage, 3.5 kV; capillary temperature, 340 $^\circ\text{C}$; S-lens RF level, 90; auxiliary gas heater temp, 35 $^\circ\text{C}$. Collected spectra were deconvoluted using the ReSpect algorithm (Protein Deconvolution 2.0; Thermo Scientific).

Data availability.

The atomic coordinates and structure factors for TrpAB structures have been deposited in the Protein Data Bank under accession codes [5TCF](#) ($\alpha^0\beta^0$), [5TCG](#) ($\alpha^0\beta^C$), [5TCI](#) ($\alpha^0\beta^O$ -BRD4592), [5TCJ](#) ($\alpha^0\beta^C$ -BRD4592), [5TCH](#) ($\alpha\text{G66V}^0\beta^0$).

Supplementary Material

Refer to Web version on PubMed Central for supplementary material.

Acknowledgments

We thank J. Gomez, M. Serrano-Wu, and B. Hubbard for helpful discussion. We would also like to thank S. Minami for assistance with *in vivo* studies. This work was supported by the Broad Institute Tuberculosis donor group, the Pershing Square Foundation, the Bill and Melinda Gates Foundation (grant OPP1032518 to S.L.S.), the National Institute of Allergy and Infectious Diseases, National Institutes of Health, Department of Health and Human

Services (HHSN272200700058C and HHSN272201200026C to A.J.) and the US Department of Energy, Office of Biological and Environmental Research (contract DE-AC02-06CH11357, A.J.). For this work, the University of Chicago is a subgrantee of Structural Genomics Consortium under a Bill and Melinda Gates Foundation grant for the Structure-Guided Drug Discovery Coalition (A.J. and K.M.).

References

1. WHO. Global Tuberculosis Report 2015 (World Health Organization, Geneva, Switzerland, 2015).
2. Zumla A, Nahid P & Cole ST Advances in the development of new tuberculosis drugs and treatment regimens. *Nat. Rev. Drug Discov* 12, 388–404 (2013). [PubMed: 23629506]
3. Mdluli K, Kaneko T & Upton A The tuberculosis drug discovery and development pipeline and emerging drug targets. *Cold Spring Harb. Perspect. Med* 5, a021154 (2015). [PubMed: 25635061]
4. Katsuno K et al. Hit and lead criteria in drug discovery for infectious diseases of the developing world. *Nat. Rev. Drug Discov* 14, 751–758 (2015). [PubMed: 26435527]
5. Andries K et al. A diarylquinoline drug active on the ATP synthase of *Mycobacterium tuberculosis*. *Science* 307, 223–227 (2005). [PubMed: 15591164]
6. Matsumoto M et al. OPC-67683, a nitro-dihydro-imidazooxazole derivative with promising action against tuberculosis *in vitro* and in mice. *PLoS Med* 3, e466 (2006). [PubMed: 17132069]
7. Manjunatha U, Boshoff HIM & Barry CE The mechanism of action of PA-824: novel insights from transcriptional profiling. *Commun. Integr. Biol* 2, 215–218 (2009). [PubMed: 19641733]
8. Stanley SA et al. Identification of novel inhibitors of *M. tuberculosis* growth using whole cell based high-throughput screening. *ACS Chem. Biol* 7, 1377–1384 (2012). [PubMed: 22577943]
9. Grzegorzewicz AE et al. Inhibition of mycolic acid transport across the *Mycobacterium tuberculosis* plasma membrane. *Nat. Chem. Biol* 8, 334–341 (2012). [PubMed: 22344175]
10. Christophe T et al. High content screening identifies decaprenylphosphoribose 2' epimerase as a target for intracellular antimycobacterial inhibitors. *PLoS Pathog* 5, e1000645 (2009). [PubMed: 19876393]
11. Stanley SA et al. Diarylcoumarins inhibit mycolic acid biosynthesis and kill *Mycobacterium tuberculosis* by targeting FadD32. *Proc. Natl. Acad. Sci. USA* 110, 11565–11570 (2013). [PubMed: 23798446]
12. Wilson R et al. Antituberculosis thiophenes define a requirement for Pks13 in mycolic acid biosynthesis. *Nat. Chem. Biol* 9, 499–506 (2013). [PubMed: 23770708]
13. Dunn MF Allosteric regulation of substrate channeling and catalysis in the tryptophan synthase bienzyme complex. *Arch. Biochem. Biophys* 519, 154–166 (2012). [PubMed: 22310642]
14. Dunn MF et al. The tryptophan synthase bienzyme complex transfers indole between the α - and β -sites via a 25–30 Å long tunnel. *Biochemistry* 29, 8598–8607 (1990). [PubMed: 2271543]
15. Anderson KS, Miles EW & Johnson KA Serine modulates substrate channeling in tryptophan synthase. A novel intersubunit triggering mechanism. *J. Biol. Chem* 266, 8020–8033 (1991). [PubMed: 1902468]
16. Niks D et al. Allostery and substrate channeling in the tryptophan synthase bienzyme complex: evidence for two subunit conformations and four quaternary states. *Biochemistry* 52, 6396–6411 (2013). [PubMed: 23952479]
17. Merino E, Jensen RA & Yanofsky C Evolution of bacterial trp operons and their regulation. *Curr. Opin. Microbiol* 11, 78–86 (2008). [PubMed: 18374625]
18. Akashi H & Gojobori T Metabolic efficiency and amino acid composition in the proteomes of *Escherichia coli* and *Bacillus subtilis*. *Proc. Natl. Acad. Sci. USA* 99, 3695–3700 (2002). [PubMed: 11904428]
19. Ngo H et al. Synthesis and characterization of allosteric probes of substrate channeling in the tryptophan synthase bienzyme complex. *Biochemistry* 46, 7713–7727 (2007). [PubMed: 17559195]
20. Lane AN & Kirschner K The catalytic mechanism of tryptophan synthase from *Escherichia coli*. Kinetics of the reaction of indole with the enzyme–lserine complexes. *Eur. J. Biochem* 129, 571–582 (1983). [PubMed: 6402362]

21. Zhang YJ et al. Tryptophan biosynthesis protects mycobacteria from CD4 T-cell-mediated killing. *Cell* 155, 1296–1308 (2013). [PubMed: 24315099]
22. Burke MD & Schreiber SL A planning strategy for diversity-oriented synthesis. *Angew. Chem. Int. Ed. Engl* 43, 46–58 (2004). [PubMed: 14694470]
23. Koul A et al. Delayed bactericidal response of *Mycobacterium tuberculosis* to bedaquiline involves remodelling of bacterial metabolism. *Nat. Commun* 5, 3369 (2014). [PubMed: 24569628]
24. Creighton TE A steady-state kinetic investigation of the reaction mechanism of the tryptophan synthetase of *Escherichia coli*. *Eur. J. Biochem* 13, 1–10 (1970). [PubMed: 4909097]
25. Copeland RA Evaluation of Enzyme Inhibition in Drug Discovery 2nd edn (John Wiley & Sons, 2013).
26. Kirschner K, Wiskocil RL, Foehn M & Rezeau L The tryptophan synthase from *Escherichia coli*. An improved purification procedure for the α -subunit and binding studies with substrate analogues. *Eur. J. Biochem* 60, 513–523 (1975). [PubMed: 1107044]
27. Hilario E et al. Visualizing the tunnel in tryptophan synthase with crystallography: insights into a selective filter for accommodating indole and rejecting water. *Biochim. Biophys. Acta* 1864, 268–279 (2016). [PubMed: 26708480]
28. Spyraakis F, Raboni S, Cozzini P, Bettati S & Mozzarelli A Allosteric communication between α and β subunits of tryptophan synthase: modelling the open-closed transition of the α subunit. *Biochim. Biophys. Acta* 1764, 1102–1109 (2006). [PubMed: 16737856]
29. Ogasahara K, Hiraga K, Ito W, Miles EW & Yutani K Origin of the mutual activation of the α and β subunits in the $\alpha_2\beta_2$ complex of tryptophan synthase. Effect of alanine or glycine substitutions at proline residues in the α subunit. *J. Biol. Chem* 267, 5222–5228 (1992). [PubMed: 1544905]
30. Rowlett R et al. Mutations in the contact region between the α and β subunits of tryptophan synthase alter subunit interaction and intersubunit communication. *Biochemistry* 37, 2961–2968 (1998). [PubMed: 9485448]
31. Harris RM, Ngo H & Dunn MF Synergistic effects on escape of a ligand from the closed tryptophan synthase holoenzyme complex. *Biochemistry* 44, 16886–16895 (2005). [PubMed: 16363802]
32. Parish T Starvation survival response of *Mycobacterium tuberculosis*. *J. Bacteriol* 185, 6702–6706 (2003). [PubMed: 14594845]
33. Swaim LE et al. *Mycobacterium marinum* infection of adult zebrafish causes caseating granulomatous tuberculosis and is moderated by adaptive immunity. *Infect. Immun* 74, 6108–6117 (2006). [PubMed: 17057088]
34. Hess I & Boehm T Intravital imaging of thymopoiesis reveals dynamic lympho-epithelial interactions. *Immunity* 36, 298–309 (2012). [PubMed: 22342843]
35. Wolf AJ et al. Initiation of the adaptive immune response to *Mycobacterium tuberculosis* depends on antigen production in the local lymph node, not the lungs. *J. Exp. Med* 205, 105–115 (2008). [PubMed: 18158321]
36. Peracchi A & Mozzarelli A Exploring and exploiting allostery: models, evolution, and drug targeting. *Biochim. Biophys. Acta* 1814, 922–933 (2011). [PubMed: 21035570]
37. Murima P, McKinney JD & Pethe K Targeting bacterial central metabolism for drug development. *Chem. Biol* 21, 1423–1432 (2014). [PubMed: 25442374]
38. DeLaBarre B, Hurov J, Cianchetta G, Murray S & Dang L Action at a distance: allostery and the development of drugs to target cancer cell metabolism. *Chem. Biol* 21, 1143–1161 (2014). [PubMed: 25237859]
39. Chen Y-NP et al. Allosteric inhibition of SHP2 phosphatase inhibits cancers driven by receptor tyrosine kinases. *Nature* 535, 148–152 (2016). [PubMed: 27362227]
40. Kasbekar M et al. Selective small molecule inhibitor of the *Mycobacterium tuberculosis* fumarate hydratase reveals an allosteric regulatory site. *Proc. Natl. Acad. Sci. USA* 113, 7503–7508 (2016). [PubMed: 27325754]
41. Nussinov R & Tsai C-J Allostery in disease and in drug discovery. *Cell* 153, 293–305 (2013). [PubMed: 23582321]

42. Turner KH, Wessel AK, Palmer GC, Murray JL & Whiteley M Essential genome of *Pseudomonas aeruginosa* in cystic fibrosis sputum. *Proc. Natl. Acad. Sci. USA* 112, 4110–4115 (2015). [PubMed: 25775563]
43. D'Elia MA, Pereira MP & Brown ED Are essential genes really essential? *Trends Microbiol* 17, 433–438 (2009). [PubMed: 19765999]
44. Lee SA et al. General and condition-specific essential functions of *Pseudomonas aeruginosa*. *Proc. Natl. Acad. Sci. USA* 112, 5189–5194 (2015). [PubMed: 25848053]
45. Cornish-Bowden A Why is uncompetitive inhibition so rare? A possible explanation, with implications for the design of drugs and pesticides. *FEBS Lett* 203, 3–6 (1986). [PubMed: 3720956]
46. Kim Y et al. High-throughput protein purification and quality assessment for crystallization. *Methods* 55, 12–28 (2011). [PubMed: 21907284]
47. Eschenfeldt WH, Lucy S, Millard CS, Joachimiak A & Mark ID A family of LIC vectors for high-throughput cloning and purification of proteins. *Methods Mol. Biol* 498, 105–115 (2009). [PubMed: 18988021]
48. Klock HE & Lesley SA The Polymerase Incomplete Primer Extension (PIPE) method applied to high-throughput cloning and site-directed mutagenesis. *Methods Mol. Biol* 498, 91–103 (2009). [PubMed: 18988020]
49. Brzovi PS, Ngo K & Dunn MF Allosteric interactions coordinate catalytic activity between successive metabolic enzymes in the tryptophan synthase holoenzyme complex. *Biochemistry* 31, 3831–3839 (1992). [PubMed: 1567839]
50. Minor W, Cymborowski M, Otwinowski Z & Chruszcz M HKL-3000: the integration of data reduction and structure solution—from diffraction images to an initial model in minutes. *Acta Crystallogr. D Biol. Crystallogr* 62, 859–866 (2006). [PubMed: 16855301]
51. French S & Wilson K On the treatment of negative intensity observations. *Acta Crystallogr. A* 34, 517–525 (1978).
52. Padilla JE & Yeates TO A statistic for local intensity differences: robustness to anisotropy and pseudo-centering and utility for detecting twinning. *Acta Crystallogr. D Biol. Crystallogr* 59, 1124–1130 (2003). [PubMed: 12832754]
53. Winn MD et al. Overview of the CCP4 suite and current developments. *Acta Crystallogr. D Biol. Crystallogr* 67, 235–242 (2011). [PubMed: 21460441]
54. McCoy AJ Solving structures of protein complexes by molecular replacement with *Phaser*. *Acta Crystallogr. D Biol. Crystallogr* 63, 32–41 (2007). [PubMed: 17164524]
55. Adams PD et al. *PHENIX*: a comprehensive Python-based system for macromolecular structure solution. *Acta Crystallogr. D Biol. Crystallogr* 66, 213–221 (2010). [PubMed: 20124702]
56. Emsley P & Cowtan K Coot: model-building tools for molecular graphics. *Acta Crystallogr. D Biol. Crystallogr* 60, 2126–2132 (2004). [PubMed: 15572765]
57. Murshudov GN, Vagin AA & Dodson EJ Refinement of macromolecular structures by the maximum-likelihood method. *Acta Crystallogr. D Biol. Crystallogr* 53, 240–255 (1997). [PubMed: 15299926]
58. Chwastyk M, Jaskolski M & Cieplak M Structure-based analysis of thermodynamic and mechanical properties of cavity-containing proteins—case study of plant pathogenesis-related proteins of class 10. *FEBS J* 281, 416–429 (2014). [PubMed: 24206126]
59. Pettersen EF et al. UCSF Chimera—a visualization system for exploratory research and analysis. *J. Comput. Chem* 25, 1605–1612 (2004). [PubMed: 15264254]
60. Nüsslein-Volhard C & Dahm R *Zebrafish: A Practical Approach* (Oxford University Press, 2002).

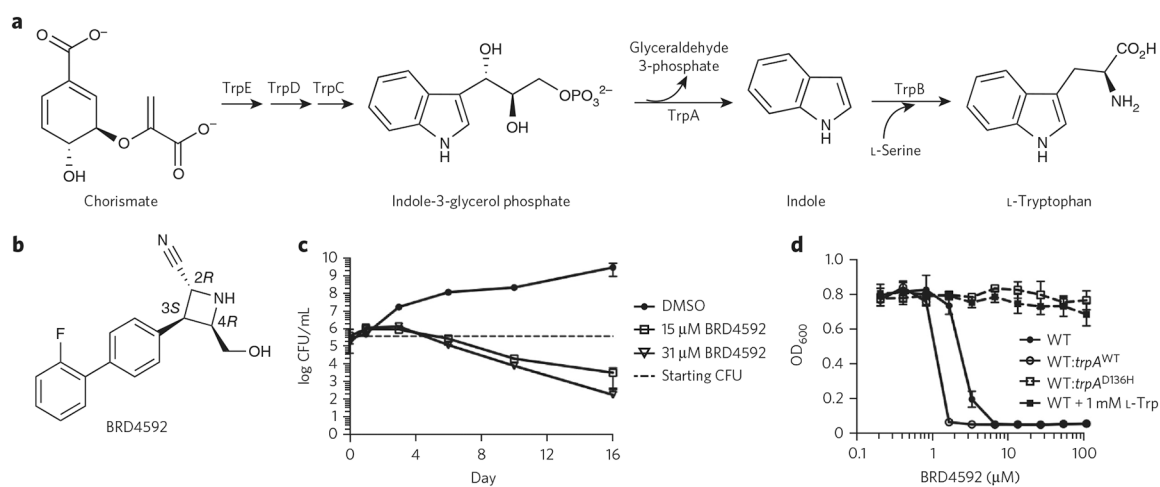


Figure 1 | BRD4592 activity against Mtb.

(a) L-Trp biosynthesis pathway. **(b)** Chemical structure of BRD4592. **(c)** Survival of Mtb grown in rich medium containing BRD4592 (15 μM or 31 μM) or DMSO (control; data are mean ± s.d. for 3 biological replicates and are representative of 3 independent experiments). **(d)** Effect of BRD4592 concentration on growth (OD₆₀₀) of WT Mtb with or without 1 mM L-Trp supplementation and WT Mtb with an episomal copy of WT or mutant *trpA* (WT: *trpA*^{WT} or WT: *trpA*^{D136H}, respectively). Data are mean ± s.d. for 4 replicates and are representative of 3 independent experiments.

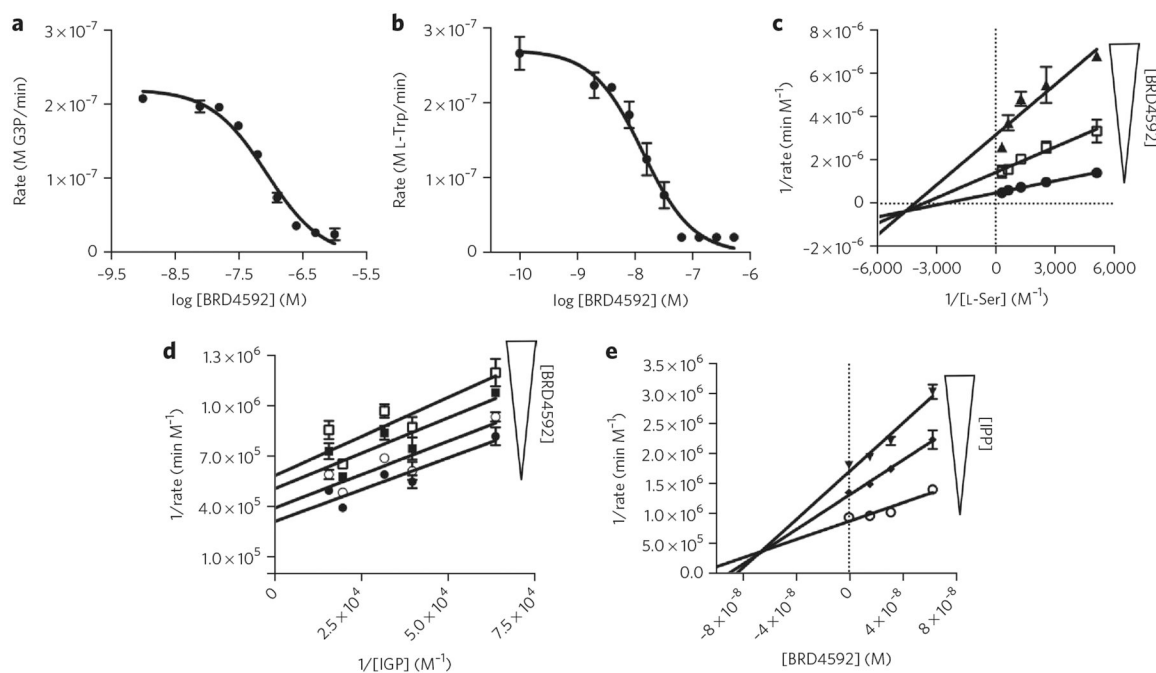


Figure 2 | BRD4592 inhibition of TrpAB *in vitro*.

(a) TrpAB G3P production from IGP and L-Ser vs. BRD4592 concentration. (b) Mtb TrpAB L-Trp production from indole and L-Ser vs. BRD4592 concentration. (c,d) Double reciprocal plot of 1/rate vs. 1/L-Ser (c) or 1/IGP concentration (d) at various BRD4592 concentrations. (e) 1/rate vs. BRD4592 concentration measured over varying concentrations of IGP-mimetic IPP. Data are mean \pm s.d. for 3 technical replicates and are representative of at least 3 independent experiments.

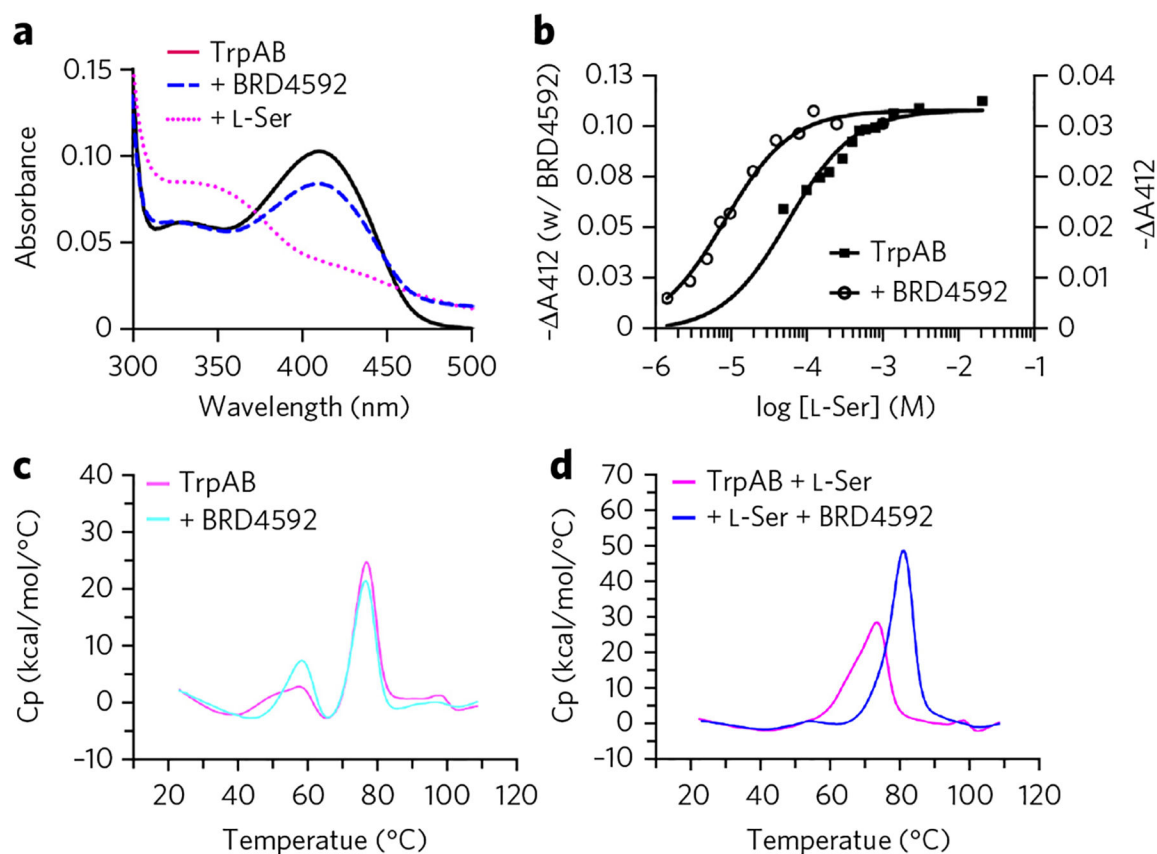


Figure 3 | BRD4592 stabilizes closed, active states of the β -subunit.

(a) Absorbance spectrum of Mtb TrpAB with BRD4592 alone or with L-Ser. The peaks at 412 nm and 350 nm are attributed to the $E_{A,int}$ state and the E_{AA} state, respectively. Data are representative of 3 independent experiments. (b) Change in TrpAB absorbance at 412 nm vs. L-Ser concentration. Data are representative of 3 independent experiments. (c,d) DSC of TrpAB (c) or TrpAB plus L-Ser (d) with (blue) or without (pink) BRD4592. With L-Ser $T_m = 73.5 \pm 1.0$ $^{\circ}\text{C}$ without BRD4592 and 81.6 ± 0.2 $^{\circ}\text{C}$ with BRD4592; data are representative of 4 (TrpAB) or 2 (TrpAB + BRD4592) independent experiments. T_m values are mean \pm s.e.m.

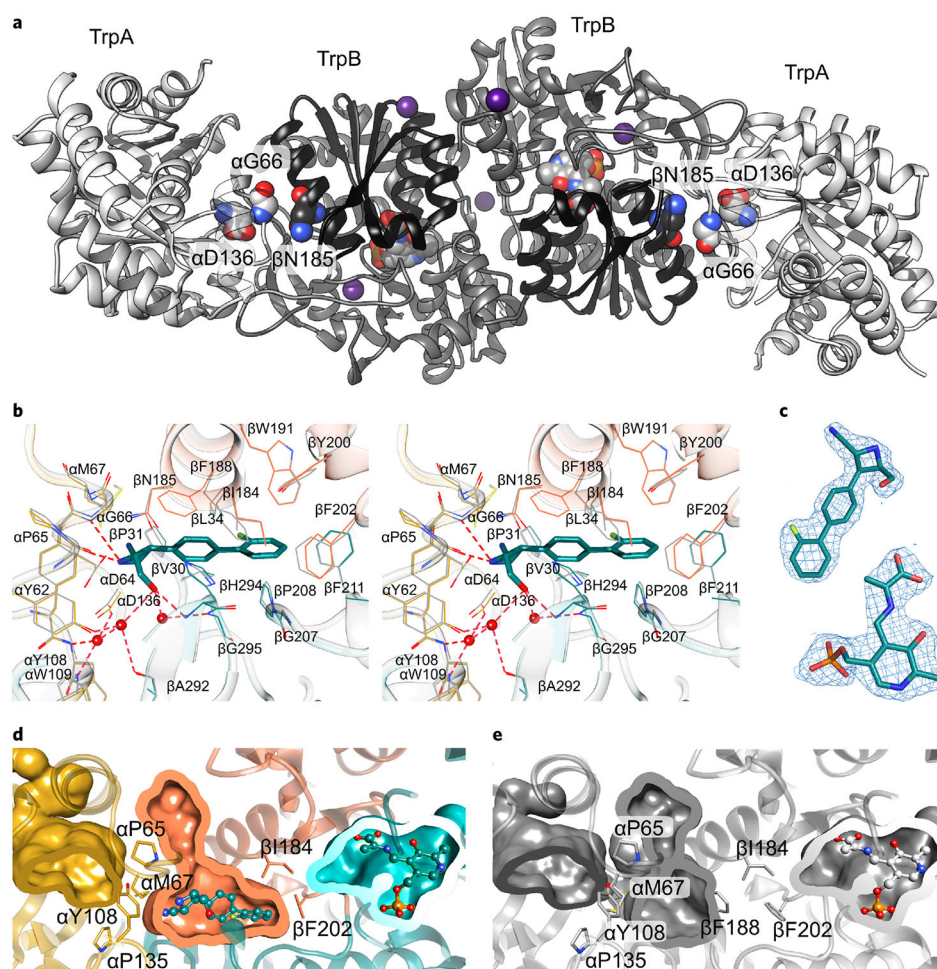


Figure 4 | Crystal structures of Mtb TrpAB.

(a) The overall structure of Mtb TrpAB with L-Ser ($\alpha^O\beta^C$, E_{AA}). The α -subunit is shown in light gray and the β -subunit in dark gray, with the COMM domain in black. The aminoacrylate adducts, positions of BRD4592 resistance mutations, and cesium ions (purple) are shown as spheres. (b) Stereo view of BRD4592 binding to $\alpha^O\beta^C$. The α -subunit is shown in yellow, the β -subunit in cyan, and the COMM domain in orange. Hydrogen bonds are shown as dashed lines, and water molecules as spheres. For reference, the BRD4592 binding site of $\alpha^O\beta^C$ without BRD4592 is superposed (gray). (c) $2DF_0 - mF_0$ electron density maps contoured at 1.2σ for BRD4592 and the aminoacrylate as seen in the $\alpha^O\beta^C$ -BRD4592 structure. (d) Pockets in the $\alpha^O\beta^C$ -BRD4592 structure. The α -pocket is shown in yellow, the β -pocket (with aminoacrylate-PLP adduct) in cyan, and inhibitor-binding pocket at the α - β interface in orange. Residues at pocket-pocket interfaces are shown. (e) Pockets in $\alpha^O\beta^C$ with no BRD4592 bound, shown as in d.

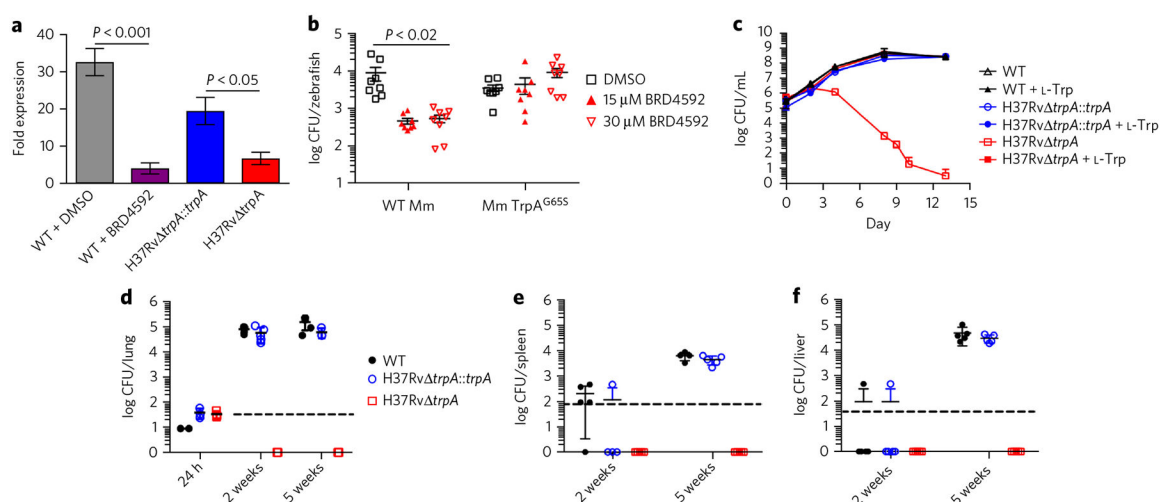


Figure 5 | TrpAB is required for survival of Mtb in various conditions.

(a) Fold expansion (day 3 CFU/day 0 CFU) of H37Rv *trpA*, H37Rv *trpA::trpA*, DMSO-treated (control) and BRD4592-treated WT Mtb in J774 macrophages. *P* values determined by unpaired two-tailed *t*-test (mean \pm s.e.m. for 4 biological replicates; representative of 3 independent experiments). (b) Effect of BRD4592 on *M. marinum* in zebrafish embryos and larvae following 5 d of treatment. Data are representative of 2 independent experiments; $n = 8$ zebrafish per condition; *P* values determined by two-way ANOVA and Turkey's multiple comparison test. (c) Growth of WT Mtb, H37Rv *trpA*, and H37Rv *trpA::trpA* in rich medium with and without L-Trp. Data are mean \pm s.d. for 3 biological replicates and representative of 3 independent experiments. (d–f) Survival of WT Mtb, H37Rv *trpA*, and H37Rv *trpA::trpA* in C57BL/6 mouse lung (d), spleen (e) and liver (f) ($n = 3$ mice (24 h) or 5 mice (2 and 5 weeks) per strain).